EM Modeling of Far-Field Radiation Patterns for Antennas on the GMA-TT UAV

Anne I. Mackenzie*
NASA Langley Research Center, Hampton, VA USA 23681-0001

ABSTRACT

To optimize communication with the Generic Modular Aircraft T-Tail (GMA-TT) unmanned aerial vehicle (UAV), electromagnetic (EM) simulations have been performed to predict the performance of two antenna types on the aircraft. Simulated far-field radiation patterns tell the amount of power radiated by the antennas and the aircraft together, taking into account blockage by the aircraft as well as radiation by conducting and dielectric portions of the aircraft. With a knowledge of the polarization and distance of the two communicating antennas, e.g. one on the UAV and one on the ground, and the transmitted signal strength, a calculation may be performed to find the strength of the signal travelling from one antenna to the other and to check that the transmitted signal meets the receiver system requirements for the designated range. In order to do this, the antenna frequency and polarization must be known for each antenna, in addition to its design and location. The permittivity, permeability, and geometry of the UAV components must also be known. The full-wave method of moments solution produces the appropriate dBi radiation pattern in which the received signal strength is calculated relative to that of an isotropic radiator.

Keywords: UAV, electromagnetic simulation, antenna placement, far-field radiation patterns

1. INTRODUCTION

When intelligence-surveillance-reconnaissance (ISR) functions are performed by a UAV, a number of antennas must be placed on the UAV to perform the various functions related to both transmitting data and flying the aircraft. Although the surveillance sensors performing the UAV's primary mission may themselves use optical frequencies, the UAV will have to communicate its data and other information back to a collection station via lower frequencies in the MHz to GHz range. It is therefore necessary to select a number of appropriate antennas and locate them on the UAV where they can best perform their functions without detriment to the aerodynamic or structural properties of the UAV. This paper concerns the electromagnetic simulation of antennas on a NASA research UAV called the GMA-TT. The reasoning and methods employed here may be applied to any UAV.

In order to achieve the best performance from all of the required antennas, it is recommended to simulate the antenna far-field radiation patterns with the antennas situated on the aircraft. Why do we model radiation patterns? The primary reason for this is to choose the antenna locations on the UAV so that the desired communication is maintained with corresponding antennas, be they on the ground, on a satellite, or elsewhere. Once an antenna is situated on a UAV, the antenna and UAV both radiate energy and the radiation pattern will be different from that of the antenna in free space. Through simulation, we can find a suitable location from which the signal is not blocked and it will reach the receiving antenna regardless of the UAV's direction or attitude. A second reason for electromagnetic simulation is to weigh the benefits of the different antenna types available. Two types that will be discussed here are blade and conformal antennas.

2. THE AIRCRAFT: GMA-TT UAV

2.1 Description of the GMA-TT

The GMA-TT is a UAV designed and built by Area-I [1] and operated by the NASA Langley Airborne Subscale Transport Aircraft Research (AirSTAR) Program [2]. The UAV is a 15.8% scale model of a generic regional transport jet with swept wings and a T-tail. The intended purpose of the dynamically scaled UAV is to fly in upset conditions so

*a.i.mackenzie-1@nasa.gov; phone 1 757 864-1820; fax 1 757 864-7975

that flight data may be gathered to characterize the response of a similar full-scale aircraft. The GMA-TT is approximately 17 feet long with a 12-foot wingspan. The body, wings, and tail of the aircraft are covered with a carbon fiber-epoxy resin composite. Testing by the Langley Electromagnetics & Sensors Branch found the outer skin to be highly reflective, with reflectivity equal to 94% at S-band. Drawings of the GMA-TT are shown in Fig. 1. For simulation purposes, the radio frequency-transparent winglets were omitted and the UAV was drawn with landing gear up in some cases and down in other cases. The x,y,z axes were drawn as indicated relative to the aircraft for all simulations. Simulation results are reported in terms of angular measurements defined with respect to the UAV.

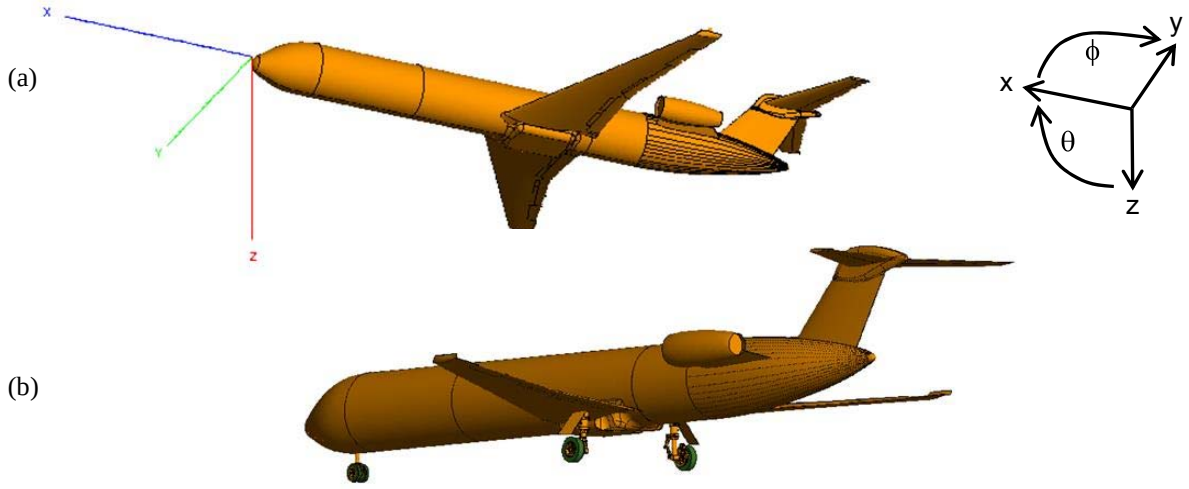

Figure 1. Simplified GMA-TT models used in simulation. (a) Landing gear up (b) Landing gear down.

2.2 Functions performed by antennas on the GMA-TT

The various functions of antennas on the GMA-TT include the following, in order of descending frequency:

a) Video transmission: C-band, 4400.0 MHz
b) Data relay: S-band, 2465.0 MHz, 2477.5 MHz (downlink)
c) Command and control: L-band, 1804.5, 1820.0 MHz (uplink)
d) GPS: L-band, 1575.42 MHz
e) ADS-B (automatic dependent surveillance – broadcast): UHF-band, 978.0 MHz
f) CS-B (formerly flight termination system): UHF-band, 425.0 MHz

3. MODELING METHODS

The UAV and antennas were modeled using the method of moments (MOM) [3] and multilevel fast multipole method (MLFMM) in FEKO software [4]. This method allows for the electromagnetic modeling of both conductive and dielectric surfaces. Because the UAV covering was found to be highly reflective, it was modeled as a perfectly electrically conductive surface except for the rubber tires. The tires were assigned a dielectric constant of 3.2 with a loss tangent of 0.02 (relative permittivity = 3.2 - j0.02, relative permeability = 1). The aircraft was drawn in as much detail as desired, omitting the smallest mechanical parts, after which the surface currents and radiated fields produced by the antennas were calculated. The radiated electric fields are typically displayed as polar plots showing dBi gain in the three principal planes relative to the aircraft as shown in Fig. 1a: $\theta = 90°$, $\phi = 0°$, and $\phi = 90°$. The dBi gain indicates radiated power at various angles relative to that of an isotropic scatterer radiating the same total power and has been normalized to the maximum gain.

For the polar gain plots, that component of the radiated power has been selected which matches the polarization of the intended receiving antenna in order to show the strength of the signal reaching its intended destination in various directions. Note that transmitting and receiving antenna pairs may be chosen intentionally to have different polarizations, such as vertical and right hand circular polarization (RHCP), for the best match when the aircraft is in flight and its attitude will be unknown. The absolute signal strength at a given angle relative to the aircraft may be calculated by first calculating the expected strongest signal and then subtracting dB according to the gain plot. The goal is to ensure that enough signal is reaching the target antenna to be detectable by the target receiver.

4. CHARACTERISTIC PATTERNS OF ANTENNAS OVER AN INFINITE GROUND PLANE

Figures 2 and 3 show the characteristic 3-dimensional patterns of a blade and a rectangular patch antenna over an infinite, flat ground plane. The blade antenna is modeled as a quarter-wave monopole. The total gain represents the sum of the electric fields including all polarizations. These patterns will be rearranged by the presence of the aircraft, which will block, reflect, and redirect energy in an irregular pattern. It would be ideal for the research flights if the antennas were to transmit equally in all directions from the UAV. We observe that the blade antenna pattern contains a null at its center and a maximum around its circumference, while the patch antenna pattern has a maximum orthogonal to the center of the patch.

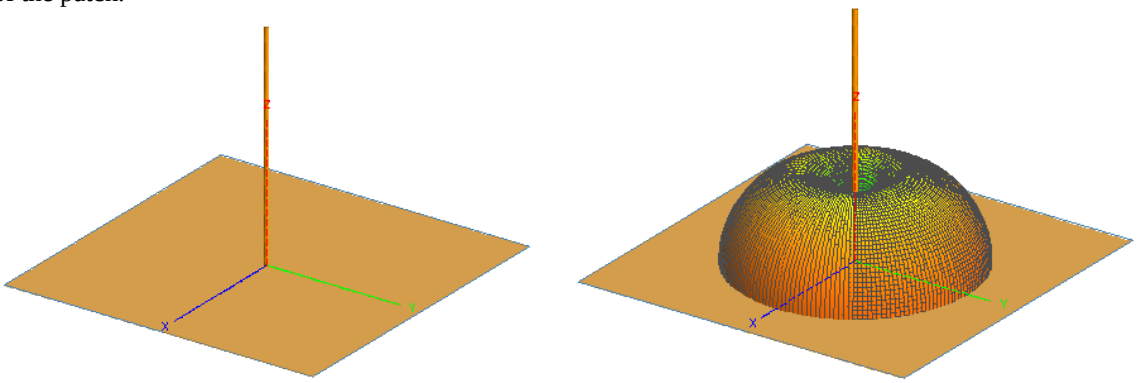

(a) (b)

Figure 2. (a) Quarter wave monopole antenna and (b) its total gain pattern over an infinite ground plane.

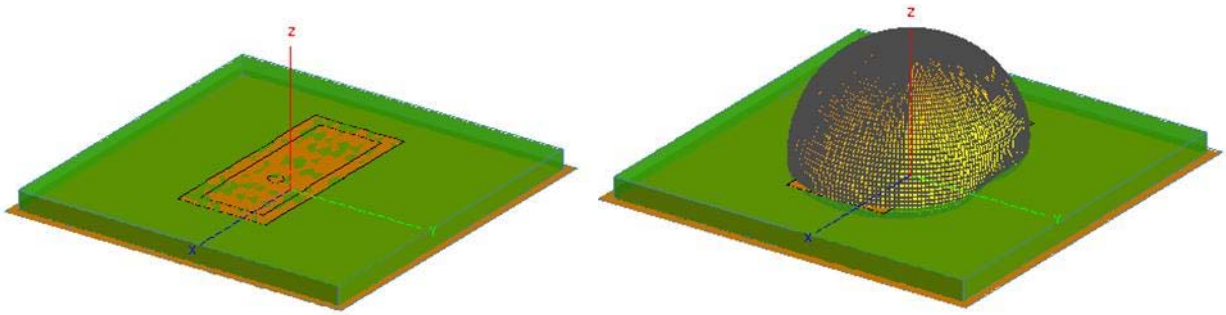

(a) (b)

Figure 3. (a) Patch antenna and (b) its total gain pattern over an infinite ground plane.

5. CALCULATED ANTENNA PATTERNS OF ANTENNAS ON THE UAV

A number of antenna patterns are shown to illustrate the nature of the blade and patch antennas. Although the following cases are possible, at this time they do not represent actual installed antennas. Above the polar plots of the following gain patterns are drawings of the UAV indicating the location of the calculated gains with respect to the UAV. Each polar plot scale varies from 0 to -30 dB. Note that some patterns assume a RHCP receiving antenna; others assume a theta, or linearly, polarized receiving antenna. The patterns apply equally well for communication in either direction between two antennas.

5.1 Blade antenna in right winglet, landing gear up versus down

A blade antenna transmitting at 2.4775 GHz is place inside the right winglet and its pattern, shown in Fig. 4, is calculated with landing gear up and down to see how much blockage occurs as a result of the landing gear.

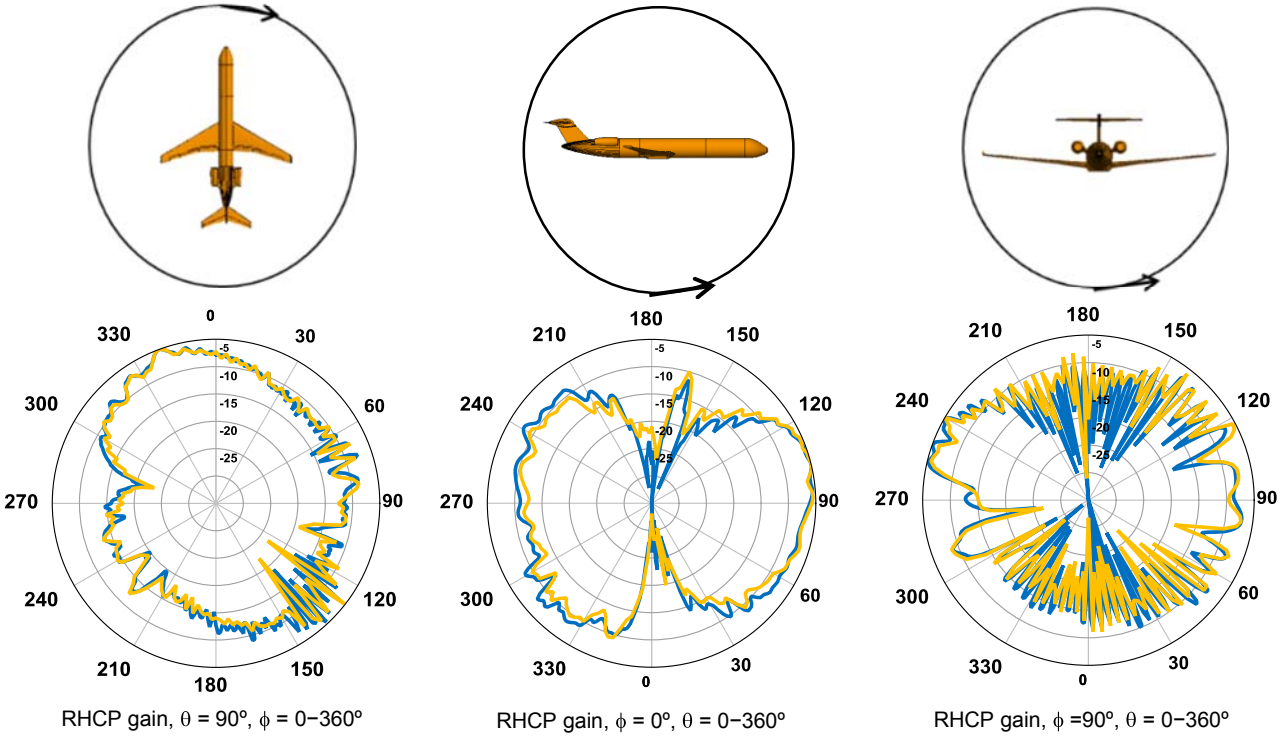

Figure 4. Radiation patterns for a blade antenna located in the right winglet, as seen by a right hand circular polarized antenna. Landing gear up ▬ Landing gear down ▬

5.2 Blade antennas in both winglets, using two S-band frequencies

Blade antennas transmitting at 2.4650 and 2.4775 GHz are placed inside the left and right winglets, respectively, and their patterns are compared in Fig. 5. The landing gear is up.

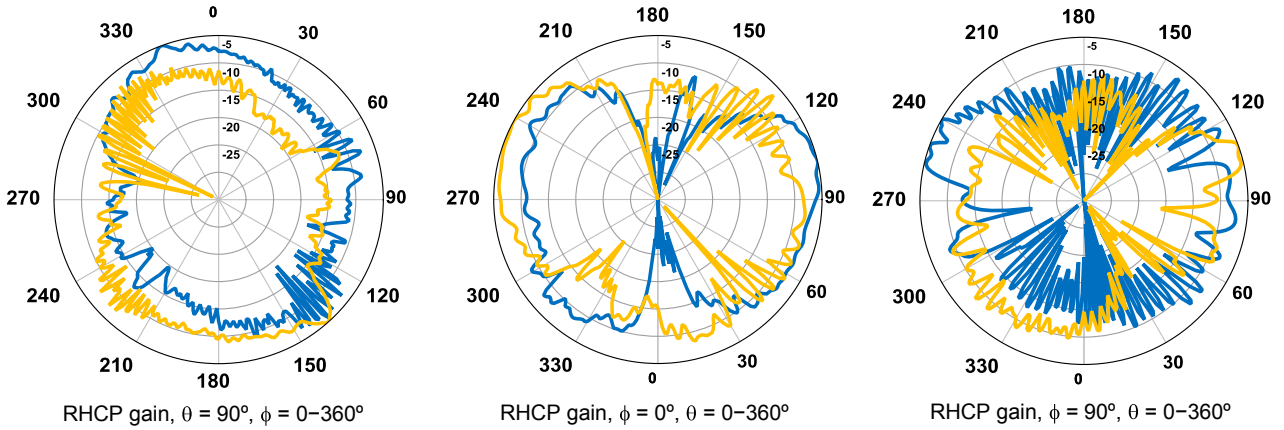

Figure 5. Radiation patterns for blade antennas located in both winglets, as seen by a right hand circular polarized antenna. Left winglet 2.4650 GHz ▬ Right winglet 2.4775 GHz ▬

5.3 Blade antennas in both winglets, using two L-band frequencies

Blade antennas transmitting at 1.8200 and 1.8055 GHz are placed inside the left and right winglets, respectively, and their patterns are compared in Fig. 6. The landing gear is up.

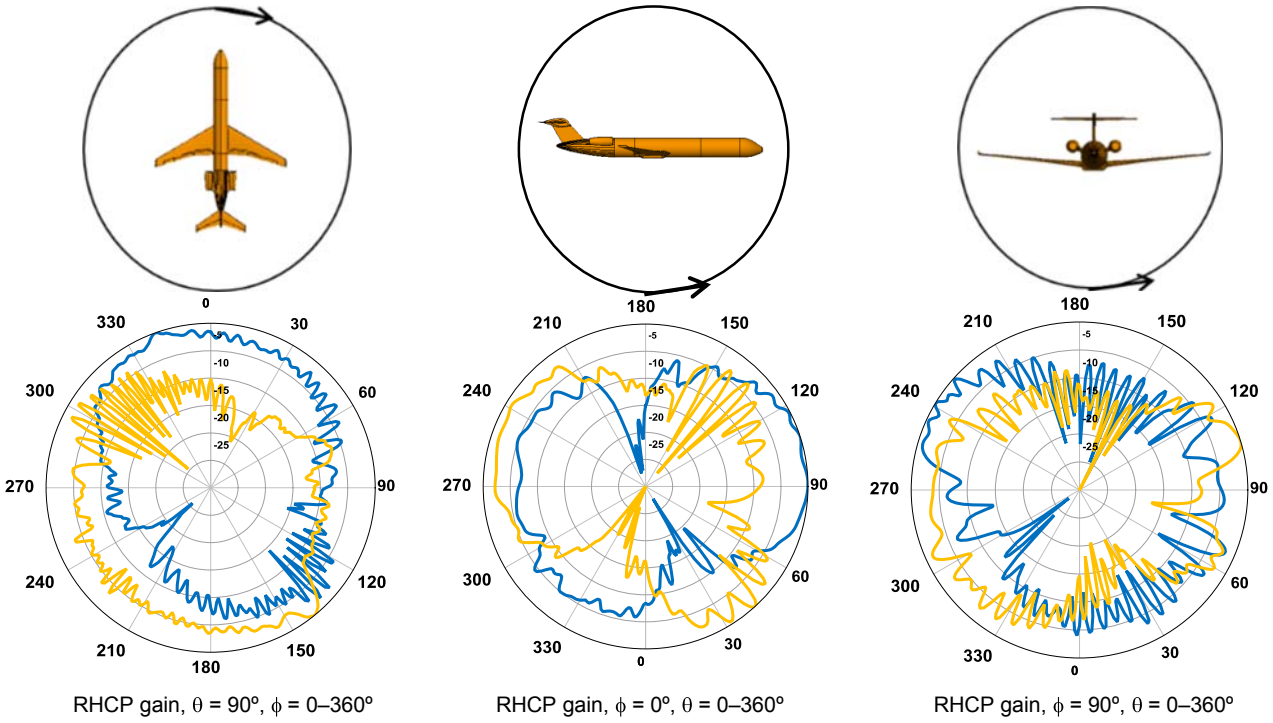

Figure 6. Radiation patterns for blade antennas located in both winglets, as seen by a right hand circular polarized antenna. Left winglet 1.8200 GHz — Right winglet 1.8055 GHz —

5.4 Patch antenna on upper left wing

A rectangular patch antenna transmitting at 425.0 MHz is located on the left wing upper surface; its radiation pattern is shown in Fig. 7. The patch location on the UAV is shown in Fig. 8a. The landing gear is up.

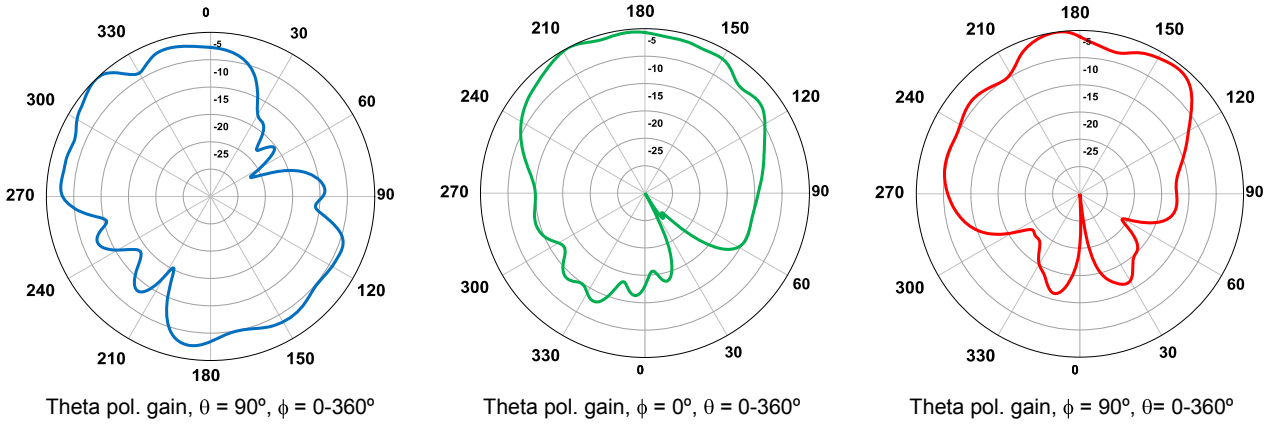

Figure 7. Radiation patterns for a patch antenna located on the left wing upper surface, as seen by a theta polarized antenna.

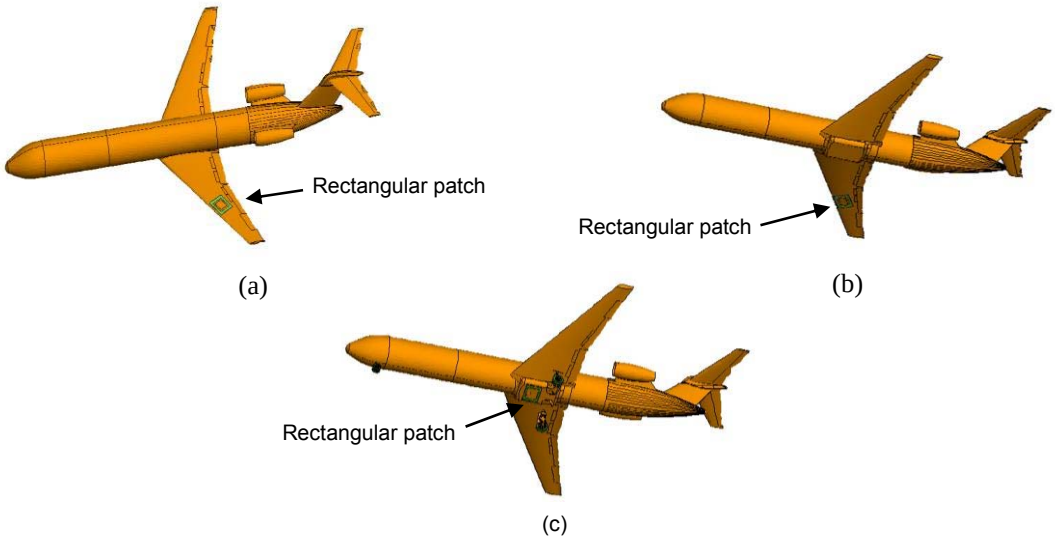

Figure 8. Location of rectangular patch on (a) left wing upper surface (b) right wing lower surface (c) fuselage lower surface.

5.5 Patch antenna on lower right wing

A rectangular patch antenna transmitting at 425.0 MHz is located on the right wing lower surface; its radiation pattern is shown in Fig. 9. The patch location on the UAV is shown in Fig. 8b. The landing gear is up.

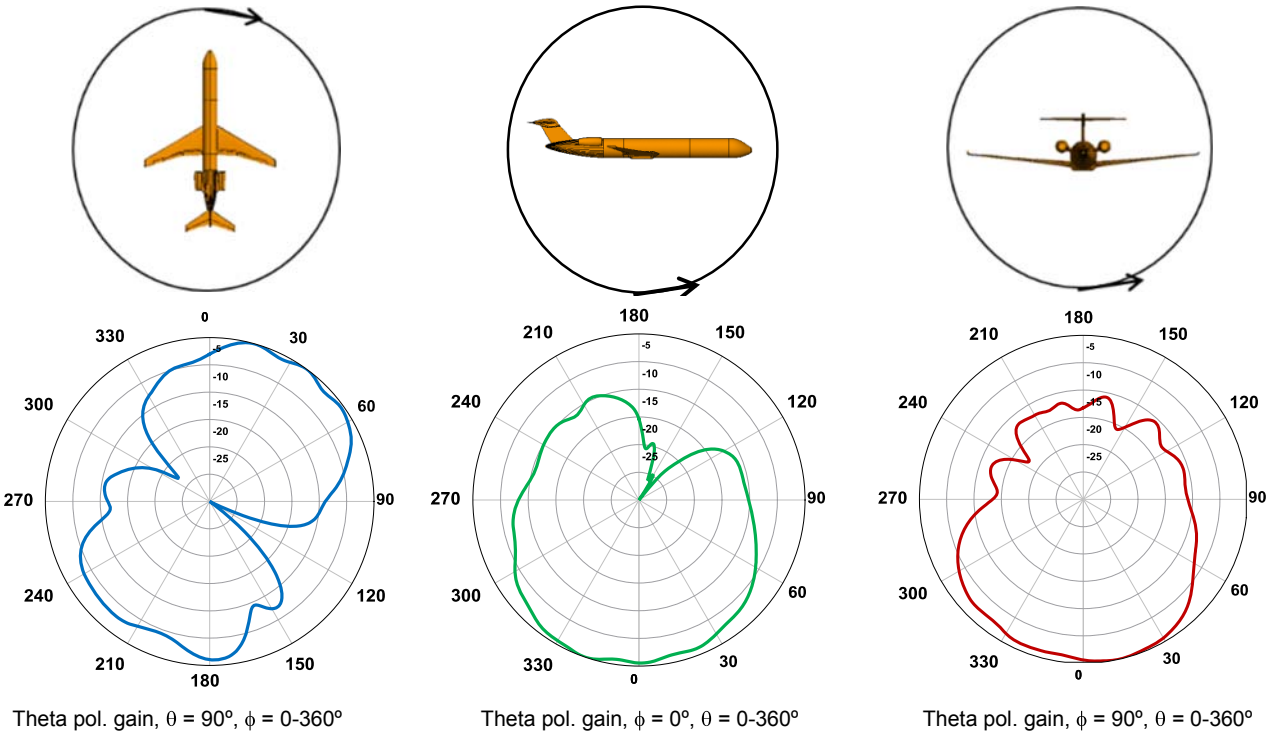

Figure 9. Radiation patterns for a patch antenna located on the right wing lower surface, as seen by a theta polarized antenna.

5.6 Patch antenna under fuselage

A rectangular patch antenna transmitting at 425.0 MHz is located on the fuselage underside; its radiation pattern is shown in Fig. 10. The patch location on the UAV is shown in Fig. 8c. The landing gear is down.

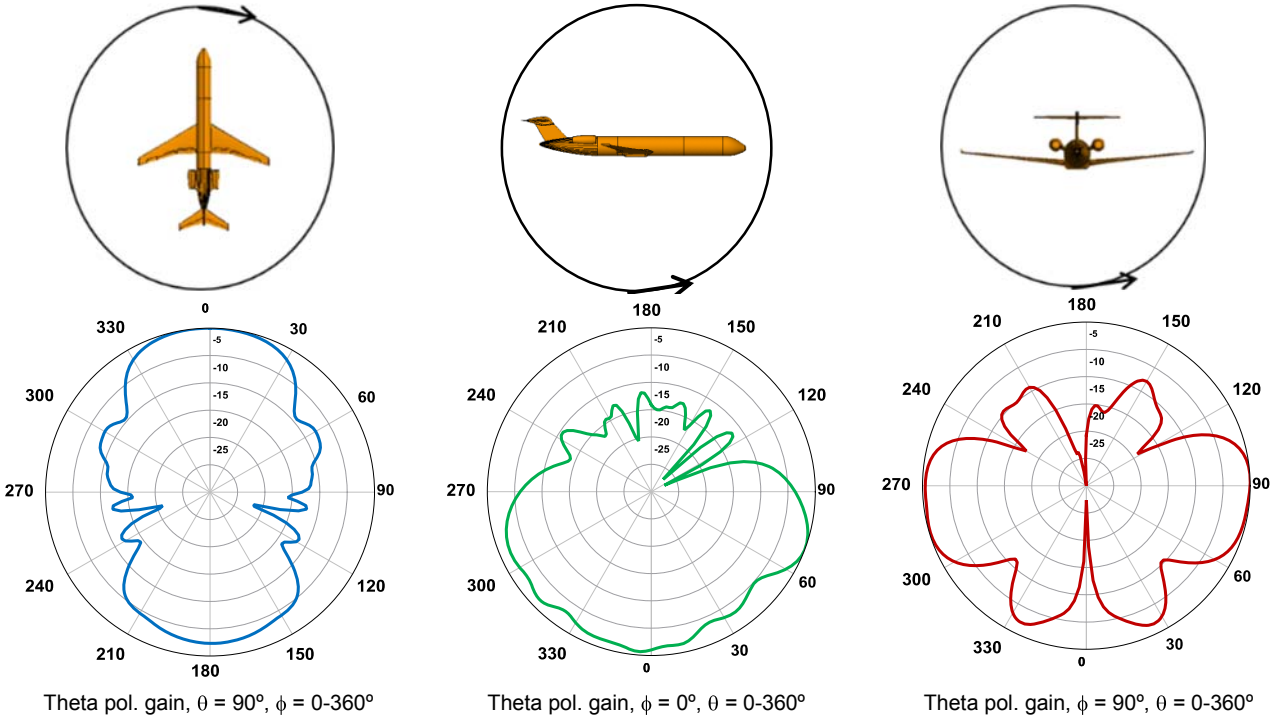

Figure 10. Radiation patterns for a patch antenna located on the fuselage underside, as seen by a theta polarized antenna.

6. DISCUSSION

With regard to the blade antenna patterns, right hand circular polarized results were selected for the plotted results because the expected receiving antenna on the Mobile Operating Station was a circular polarized dish antenna. The comparison of S-band blade antenna patterns with the UAV landing gear up versus down shows that the landing gear does not greatly affect signal transmission when the antennas are located in the winglets. With the landing gear down, the signal is about 5 dB lower at some angles beneath the aircraft but is about 2 dB higher at other angles. By adding another S-band antenna at a slightly different frequency (2.4650 versus 2.4775 GHz) in the opposite winglet, it is possible to compensate for the dropout in one signal by transmitting the same information with another signal. Use of this strategy requires that the receiver be able to detect signals at both frequencies and record the stronger one. Examination of the results for two L-band blade antennas (1.8200 and 1.8055 GHz) in the winglets shows that the lower frequencies yield slightly better coverage in all directions as compared to the S-band frequencies. Again, the signal generated by the antenna in one winglet compensates for deficiencies in the other. With the blade antenna, there tend to be weak points in the pattern directly above and below the antenna, in the case of the winglet location, directly above and below the UAV.

With regard to the patch antennas, theta (linear) polarized results were selected for the plotted results because the expected receiving antenna was linearly polarized. The patterns for patch antennas located on an upper or lower wing surface show some blockage by the aircraft body in the x-y plane. The majority of the signal radiates outward from the UAV on the same side as the patch with a smaller amount radiating from the side of the UAV opposite to the patch. In the case where the patch resides on the underside of the fuselage, a null is seen at $\theta = 0$ and 180º. This null is due to the combination of linear transmitting and receiving antennas oriented at right angles to each other. With the patch antenna, there tend to be weak points in the pattern in the plane of the antenna, at $\theta = 90$º.

7. CONCLUSION

We have discussed some of the principles involved in simulating antenna patterns to assist with antenna placement on a UAV. Examples of blade and patch antennas were used in various locations on the GMA-TT UAV. The two antenna types have different characteristic radiation patterns. It was shown that a pair of antennas may be used with slightly different frequencies, so that one signal may compensate for dropout in the other. The signal strength in any given direction depends not only on the antenna design and placement, but also on the shape and composition of the aircraft and the polarization of the remote antenna communicating with the UAV antenna. The same methods employed here may be used to simulate antenna performance on other UAV's.

ACKNOWLEDGEMENTS

This work was funded by the AirSTAR Program at the NASA Langley Research Center.

REFERENCES

[1] http://areai.aero
[2] Jordan, T. L., Foster, J. V., Bailey, R. M., and Belcastro, C. M., "AirSTAR: A UAV platform for flight dynamics and control system testing," 25th AIAA Aerodynamic Measurement Technology and Ground Testing Conference, June 5-8 2006, San Francisco, CA, AIAA Paper 2006-3307.
[3] Harrington, R. F., **[**Field Computation by Moment Methods], IEEE Press, Piscataway, NJ, 1993.
[4] https://www.feko.info